2010 IEEE-RAS International Conference on Humanoid Robots
Nashville, TN, USA, December 6-8, 2010

Weight-Adaptive Walking of the Passenger-Carrying Biped Robot, HUBO FX-1

Jung-Hoon Kim, Jung-Yup Kim, and Jun-Ho Oh

Abstract—**In a passenger-carrying walking humanoid robot, it is preferable to use the walking pattern generation and balance control method that can accommodate variable passenger weights. This is because the range of possible payloads for passenger weight is relatively wide, from zero to approximately one hundred kgf. If the variable weight is not considered, the walking performance and walking stability of the robot decrease when the passenger's weight was much heavier or lighter than the predefined passenger weight. Therefore, in this paper, the walking pattern generation and ZMP control methods are developed to adaptively cope with variable passenger weights. The walking pattern generation method using the convolution sum can effectively calculate the walking pattern for variable passenger weights since it contains the analytic function of variable mass. The ZMP controller that performs the real-time sensor feedback control is designed as state space forms where the gains can be easily changed for variable passenger weights. The experiments show that the walking performance of the proposed method is well maintained and superior to those of the non-adaptive controllers for three different payload levels.**

I. Introduction

Passenger-carrying biped robot is a practical biped robot capable of carrying a human. This robot is differentiated from the wheel-based type of vehicle, and it can be used in the welfare field as a walking wheelchair or a walking support machine that is able to the traverse stairs [1,2] and in the entertainment field as an amusing vehicle. In addition, previous research has considered this type of robot as having the potential to offer much greater mobility than that of a wheelchair [3]. The WL-16 (Waseda Leg - No.16) developed in 2003 was the world's first biped-walking robot capable of carrying a human [1,2]. Its expected use was that of a multi-purpose locomotion vehicle. By designing a leg with a 6-DOF parallel mechanism, the mechanical rigidity was increased and the weight of the structural components was decreased. The weight of this robot was 56 kgf, including the battery, and the height was approximately 1.2 m. Toyota released their "i-foot" robot in 2004, which was able to climb up and down staircases [4]. This machine was composed of serially connected rotary actuators, similar to that of the general humanoid robot, and the legs were bent toward the rear so that the passenger could ride comfortably on the robot. The height of the "i-foot" was 2.36 m, with a weight of 200 kgf. The maximum weight capacity of the passenger was 60 kgf, and the walking speed was 1.35 km/h. Subsequently, the HUBO FX-1 was first demonstrated to the public at the 2005 APEC summit, and the initial version of the control algorithm was published first in reference [5]. This robot was designed for a maximum passenger weight of 100 kgf. Our previous paper [5] described the design of the passenger-carrying biped robot and the structural vibration control of the swing leg, which is different from that of a life-size humanoid robot, as well as the experiments performed for a passenger weight of 81 kgf. Passenger- carrying biped robots are different than the general life-size humanoid robots, such as ASIMO, HRP, and HUBO, in that these have their passenger seats on the lower limbs and the unknown passenger weight is applied as an additional payload. Therefore, the mechanism for increasing the rigidity of the lower limb structure was needed to be designed [1,2] and the process for solving the structural vibration problem resulting from the weight reduction and its experimental verification was investigated [5]. In reference [5], all of the parameters for the walking patterns and online controllers were tuned for a specific passenger weight of 81 kgf. In the passenger-carrying biped robots on which passengers are able to have a variety of weights, from lighter children to heavier adults, it is very important that the walking performance does not change with passenger weight. In order to realize this objective, the walking pattern generation and online feedback controllers for biped walking must have adaptive characteristics that enable the parameters to be suitably determined for each of the variable passenger weights. Therefore, by focusing on the variable mass, which has not been covered in previous research, this paper describes the novel walking pattern generator and controllers that have been designed for variable masses.

Manuscript received June 24, 2010.

Jung-Hoon Kim is with the Yonsei University, South Korea (e-mail : junghoon@yonsei.ac.kr).

Jung-Yup Kim is with the Seoul National University of Science & Technology, South Korea (corresponding author to provide phone : +82-2-970-6355;e-mail : jyk76@snut.ac.kr).

Jun-Ho Oh is with the Korea Advanced Institute of Science and Technology, South Korea (e-mail : jhoh@kaist.ac.kr).

II. Passenger-Carrying Biped Robot, HUBO FX-1

The HUBO FX-1 is composed of two main parts: a lower body for locomotion and a cockpit for the passenger (Fig. 1). Harmonic reduction gears and AC servo motors with high capacities(400 and 800Watts) were used as actuators. The main computer, interface board, and motor drivers used to control the HUBO FX-1 are located in the cockpit. The maximum height is 1,987 mm; however, the HUBO FX-1 lowers its height by 60 mm during walking. Each leg has six degrees of freedom; hence there are 12 degrees of freedom in

total. All of the actuators were used in order to compensate for a passenger weight of 100 kgf.

Three types of sensors were developed and installed in the HUBO FX-1. The first was the three-axis force/torque sensor, located on the foot, that measures the vertical ground reaction force (up to 3000 N) and the pitching and rolling ground reaction torques (up to 320 Nm). The second sensor was the inertial sensor at the pelvis center, which is composed of three rate gyros in the roll, pitch and yaw directions and two accelerometers in the forward (x) and lateral (y) directions. The third sensor was the accelerometer at the feet, used for the vibration control of the swing leg. With these three types of sensors and AC servo motor controllers, we built a distributed control system. If a main computer sends the desired angular positions of all of the joints to an interface card stacked on the main computer, the interface card can then convert the desired angular positions into pulses and can subsequently transmit them to all of the AC servo motor controllers at the frequency of 100 Hz. The sensor data can also be received at a frequency of 100 Hz.

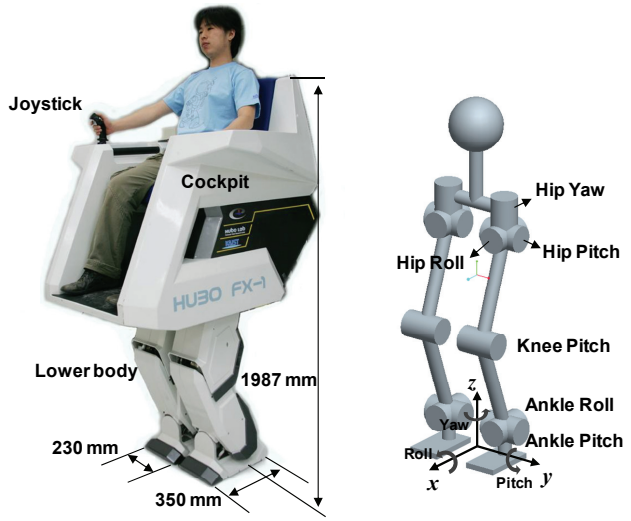

Fig. 1 Passenger-carrying biped robot HUBO FX-1

III. Adaptive Walking Pattern Generation Using Convolution Sum

An effective walking pattern generation method using the convolution sum [6] was selected for use in this research among the various methods [7,8], as this method enables the easy and accurate calculation of the walking patterns for variable passenger weights and does not require much computation power.

For the robot model, a single mass inverted pendulum model is used, and the ZMP equation can be expressed as a decoupled linear differential equation in the forward and lateral directions [6-8].

$$y_{ZMP} = y - \frac{1}{\lambda^2}\ddot{y} \quad where \quad \lambda = \sqrt{g/l} \tag{1}$$

where g is the gravitational acceleration, l is the equivalent length of the pendulum, y is the walking pattern (i.e., displacement) of the mass center in the lateral direction, and y_{ZMP} is the reference ZMP in the lateral direction, respectively. From the viewpoint of the linear system response, walking pattern generation can be regarded as a convolution of an arbitrary reference ZMP and the walking pattern for an impulse reference ZMP.

$$y[n] = \sum_{k=-\infty}^{k=\infty} u[n-k]h[k] \tag{2}$$

where $y[k]$ is the walking pattern of the mass center in the lateral direction, $u[k]$ is an arbitrary reference ZMP input in the same axis, and $h[k]$ is the walking pattern for an impulse reference ZMP. This method is similar to the calculation of a linear system response, where the solution is calculated by taking the convolution integral of the impulse response and an excitation input. Since the biped robot is modeled as a single inverted pendulum and its equation of motion is given by a linear differential equation, the principle of superposition can be applied and the convolution sum can also be used. In this method, it is only necessary to know the walking pattern solution of the ZMP equation for the impulse reference ZMP in order to calculate the trajectory that tracks an arbitrary reference ZMP. The analytic walking pattern for an impulse reference ZMP input when the impulse reference ZMP is given at $n = 0$, was derived in [6], and the convergent solution was solved in the discrete domain as follows:

$$\begin{aligned} &h[n] = h[0]\cdot e^{-|n|\lambda T} \\ &where \;\; h[0] = \frac{1}{2}(e^{\lambda T}-1)e^{-\frac{\lambda T}{2}} = \sinh\left(\frac{\lambda T}{2}\right) \end{aligned} \tag{3}$$

The walking pattern in (2) can be divided into future term and past term.

$$y[n] = y_{future}[n] + y_{past}[n] \tag{4}$$

$$\begin{aligned} where \quad y_{future}[n] &= \sum_{k=1}^{k=\infty} u[n+k-1]h[k-1] \\ &\approx \sum_{k=1}^{k=N} u[n+k-1]h[k-1] \end{aligned} \tag{5}$$

$$y_{past}[n] = \sum_{k=1}^{k=\infty} u[n-k]h[k] \tag{6}$$

In (5), the infinite weighted sum of $u[k]$ could be approximated using a sufficiently large number N for the weighted sum; however, this required sacrificing the accuracy. If N is large, the resultant ZMP is accurate, but it requires more computation power.

For the past term, the recursive form could be derived as follows:

$$\begin{aligned} &y_{past}[n] = e^{-\lambda T} y_{past}[n-1] + h[1]\cdot u[n-1] \\ &where \quad h[1] = \sinh\left(\frac{\lambda T}{2}\right)\cdot e^{-\lambda T}, \quad \lambda = \sqrt{g/l} \end{aligned} \tag{7}$$

The recursive form of the past term reduces the computation power during the process of walking pattern generation.

The walking pattern that tracks the arbitrary reference ZMP input $u[k]$ can easily be calculated using (3), (4), (5) and (7). The algorithm using the convolution sum is a novel idea in terms of a walking pattern generation method, and this paper shows its first application in a real biped robot. The proposed algorithm has a similarity with the preview control in [7], which needs a finite future reference, but the proposed algorithm does not require solving the Riccati equation to decide the preview gain and feedback gain. It has an advantage that the basic function required in walking pattern generation is analytically expressed in terms of the equivalent length l. This walking pattern generation method is suitable for variable passenger weights because of the characteristics of its equation, such as accuracy, low computation power and simplicity. These advantages were verified using a simulation in previous research [6].

Using the above algorithm, walking patterns for the variable passenger weights can be generated. The equivalent lengths for the passenger weights of 20 kgf, 40 kgf, and 60 kgf were 0.7345 m, 0.7995 m, and 0.8538 m, respectively (The calculations of the equivalent lengths will be explained in Section IV). The walking patterns for the impulse reference ZMP, $h[k]$, were obtained using (3) and are a function of the equivalent length. The final walking patterns which tracked the reference ZMP $u[k]$ were calculated by taking the convolution sum with $h[k]$ and $u[k]$, using (4), (5) and (7). When three different levels of passenger weights (20 kgf, 40 kgf, and 60 kgf) were applied, the distinct walking patterns for the same reference ZMP along the axes y and x could be plotted (Figs. 2 and 3).

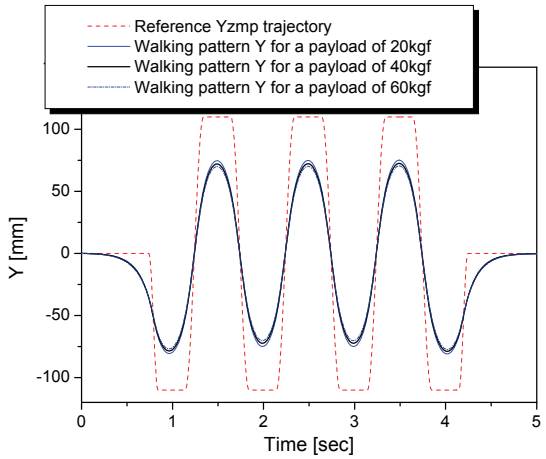

Fig. 2 Reference y_{ZMP} and walking patterns in y-direction for variable passenger weights

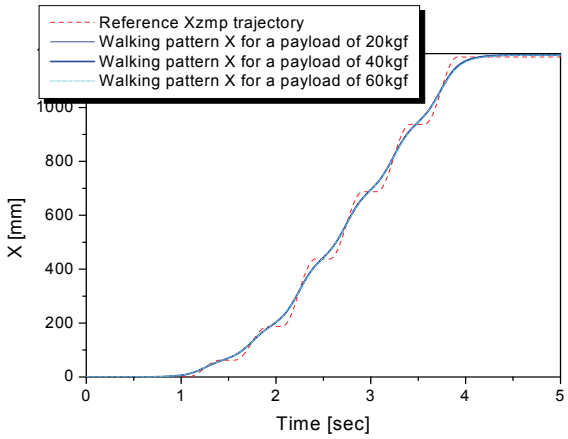

Fig. 3 Reference x_{ZMP} and walking patterns in x-direction for variable passenger weights

The step time in these figures is 1 second, and the maximum stride is 250 mm. As seen in Fig. 2, the maximum amplitude of the hip sway for a passenger weight of 20 kgf is 80.55 mm, and it decreases as the passenger weight increases. For a passenger weight of 60 kgf, the maximum value becomes 76.83 mm. In the forward walking patterns for the various payloads of Fig. 3, the maximum difference in the hip patterns along the x axis is approximately 3.5 mm.

IV. Adaptive ZMP Control

In this section, we propose a ZMP controller that is based on the simple state feedback using a direct state measurement for a fast response and easy gain switching according to passenger weight. The dynamic model of the ZMP controller is a single inverted pendulum with a flexible joint (Fig. 4). Its linearized equation of motion can be represented as follows:

$$\begin{aligned} ml^2\ddot{\theta} &= mgl\theta + \tau \\ \tau &= -K_s(\theta - u) \end{aligned}, \qquad (8)$$

where K_s is the torsional spring constant, l is the equivalent length, g is the gravitational acceleration, m is the point mass, and u and θ are the reference and actual angular positions of the joint, respectively. The torsional spring constant K_s represents the flexibility of the frame structure, because an actual biped robot oscillates back and forth or side to side when it is pushed and released backward or sideways during the single or double support phases. Here, it is important to note that K_s has no relation to passenger weight, whereas l and m are variable according to passenger weight. This means that the parameters of the equation of motion can be changed; hence, the control gain should be also changed according to the passenger weight in order to maintain the control performance.

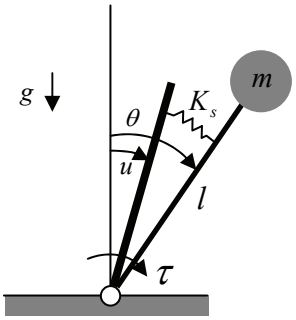

Fig. 4. Single inverted pendulum model with a flexible joint

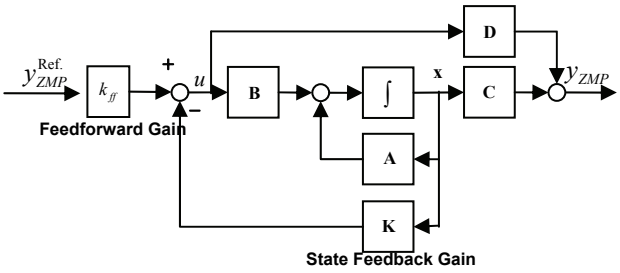

Fig. 5. Block diagrams of the proposed ZMP control

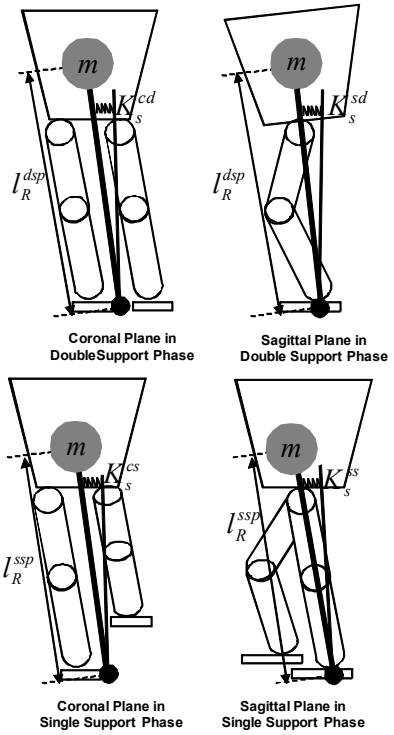

Fig. 6. Two types of l_R and four types of K_s

In Fig. 5, **A**,**B**,**C** and **D** are the state, input, output, and direct transmission matrices, respectively. As such, it became possible to much more simply express the state feedback gains as a function of m, l , and the closed loop poles. In (8), the point mass m could be measured by the force/torque sensors at the feet, and the equivalent length l could be easily calculated using the following relationships:

$$l = \frac{l_R m_R + l_P m_P}{m_R + m_P} \tag{9}$$

$$m = m_R + m_p \tag{10}$$

where m_R and m_P represent the masses of the robot (= 180 kg) and the passenger, respectively, and l_R and l_P are the equivalent lengths of the robot and its passenger. The mass of the passenger m_P can be easily calculated by subtracting the weight of the robot from the total weight, and the equivalent length of the passenger l_P was assumed to be 1.45 m, which was simply calculated by considering the height of the seat and the upper body of the passenger. On the other hand, the equivalent length of the robot l_R and the torsional spring constant K_s must be calculated simultaneously through experiments. In particular, the equivalent length of the robot l_R differs depending on the single and double support phases, and the torsional spring constant K_s can also differ depending on the single and double support phase and coronal and sagittal planes. Two types of l_R and l_P are shown in Fig. 6.

In (8), if we define the input, output, and state variables as the horizontal displacement y_h (= lu), the zero moment point y_{ZMP} (= τ /mg), and the angular position θ and velocity $\dot{\theta}$, respectively, then the state space equations and transfer function G(s) can be represented as follows:

$$\begin{aligned} \dot{\mathbf{x}} &= \mathbf{A}\mathbf{x} + \mathbf{B}y_h \\ y_{ZMP} &= \mathbf{C}\mathbf{x} + \mathbf{D}y_h \end{aligned} \tag{11}$$

where, $\mathbf{A} = \begin{bmatrix} 0 & 1 \\ \frac{g}{l} - \frac{K_s}{ml^2} & 0 \end{bmatrix}$, $\mathbf{B} = \begin{bmatrix} 0 \\ \frac{K_s}{ml^3} \end{bmatrix}$, $\mathbf{C} = \begin{bmatrix} \frac{K_s}{mg} & 0 \end{bmatrix}$, $\mathbf{D} = \begin{bmatrix} -\frac{K_s}{mgl} \end{bmatrix}$, and $\mathbf{x} = \begin{bmatrix} \theta \\ \dot{\theta} \end{bmatrix}$

$$G(s) = \frac{y_{ZMP}}{y_h} = -\frac{K_s}{mgl} \cdot \frac{s^2 - \frac{g}{l}}{s^2 + \frac{K_s}{ml^2} - \frac{g}{l}} \tag{12}$$

Using (12), it is possible to calculate the two types of equivalent lengths of robot l_R and the four types of spring constant K_s by experimentally measuring the DC gain of a step response and the natural frequency without a passenger. The following (13) and (14) show the natural frequency and DC gain derived from (12). When there is no passenger, the equivalent length l and point mass m are equal to l_R and m_R, respectively. Here, if the natural frequency ω_n and steady-state value of y_{ZMP} are experimentally measured, the

equivalent length of the robot l_R and the torsional spring constant K_s can be derived simultaneously.

$$\omega_n = \sqrt{\frac{K_s}{m_R l_R^2} - \frac{g}{l_R}} \tag{13}$$

$$y_{ZMP}(\infty) = \lim_{s \to 0} G(s) = \frac{K_s g}{m_R g l_R^2 \omega_n^2} \tag{14}$$

For each of the four cases in Fig. 6, we conducted experiments and then identified the equivalent lengths of the robot l_R and the torsional spring constant K_s of the HUBO FX-1 (Table I). The spring constant was the highest for the coronal plane in the double support phase, because the supporting width was the longest. Conversely, it was the lowest for the coronal plane in the single support phase, due to the fact that it had the shortest supporting width. The equivalent lengths of the robot for the coronal and sagittal planes in each support phase were almost identical.

TABLE I
EXPERIMENTAL IDENTIFICATION OF THE EQUIVALENT LENGTHS AND TORSIONAL SPRING CONSTANTS FOR THE FOUR CASES

	Coronal Plane	Sagittal Plane
Double Support Phase(DSP)	$l_R^{dsp} = 0.7174$ [m] $K_s^{cd} = 21998.64$ [Nm/rad]	$l_R^{dsp} = 0.7174$ [m] $K_s^{sd} = 14784.82$ [Nm/rad]
Single Support Phase(SSP)	$l_R^{ssp} = 0.655$ [m] $K_s^{cs} = 4557.15$ [Nm/rad]	$l_R^{ssp} = 0.655$ [m] $K_s^{ss} = 5774.453$ [Nm/rad]

With the equivalent lengths and torsional spring constants for four cases established, a ZMP contoller based on the state feedback in each case could be proposed :

$$y_h = -\mathbf{K}\mathbf{x} \tag{15}$$
$$where,\ \mathbf{K} = \begin{bmatrix} k_1 & k_2 \end{bmatrix}$$

Then, a characteristic equation was derived:

$$\left| s\mathbf{I} - \mathbf{A} + \mathbf{B}\mathbf{K} \right| = s^2 + \left(\frac{K_s}{ml^3} k_2 \right) s - \frac{g}{l} + \frac{K_s}{ml^2} \left(1 + \frac{k_1}{l} \right) = 0 \tag{16}$$

If the desired closed poles are defined as $s = -a \pm bj \ \ (a > 0)$ to conduct the pole placement, the state feedback gain matrix $\mathbf{K}$ becomes

$$\mathbf{K} = \begin{bmatrix} k_1 \\ k_2 \end{bmatrix} = \begin{bmatrix} \dfrac{\left[\left(a^2 + b^2 \right) + \dfrac{g}{l} \right] ml^3}{K_s} - l \\ \dfrac{2aml^3}{K_s} \end{bmatrix} \tag{17}$$

Therefore, the state feedback gain matrix can be represented as a function of m, K_s, l and the desired closed-loop poles. Since the parameters l, m, and K_s can be calculated from (9), (10) and Table I, it is easy to change the state feedback gain according to the passenger weight. Consequently, the four types of the state feedback gain matrix are designed straightforwardly.

To verify the performance of the ZMP controller, we conducted experiments with the HUBO FX-1. The closed-loop pole locations of the four cases were defined as $s = -3 \pm 3j$ by considering the suitable settling time of 1 second and a damping ratio of 0.707 in a typical second-order system. We fully pushed and released the robot to create an external disturbance and then collected the ZMP data. The external disturbances were applied to the robot in both the double and single support phases. Figures 7 (a), (b), (c), and (d) show the experimental results. In each graph, we compared the six cases. The black lines in the figures represent the results without the ZMP control. In these cases, the ZMP oscillations were sustained for a long time. The blue lines show the results when the non-adaptive ZMP control was applied to the robot with no payload. The non-adaptive ZMP control only considers a specific passenger weight, where it uses the state feedback gain with a passenger weight of zero. When there was no payload, the ZMP oscillations were effectively reduced. However, when a payload of 20 kgf was applied to the robot, the amplitudes of the ZMP oscillations increased and the settling times became longer (red lines). Conversely, when we applied the adaptive ZMP control that considers the payload of the robot, the amplitudes of the ZMP oscillations, described by the green lines, decreased and the setting times became shorter compared to the results of the non-adaptive ZMP control. Likewise, the pink and orange lines show the ZMP oscillations under non-adaptive ZMP control and adaptive ZMP control, respectively, when a payload of 40 kgf was applied. It is understood that the ZMP oscillations reduce much faster with the adaptive ZMP control. Consequently, the settling times for all cases in Fig. 7 are summarized in Tables II and III. In addition, the settling time with the non-adaptive ZMP control increased according to the payload, while the adaptive ZMP control maintained a short settling time of approximately 2 seconds regardless of the payload. Therefore, the adaptive ZMP control clearly showed a superior performance to the non-adaptive ZMP control used in our previous research.

In addition to the adaptive ZMP control, we actually proposed an adaptive landing timing control and an adaptive vibration control that also consider the variable passenger weight. Though they are not addressed in this paper, they were used to build our adaptive balance control strategy. In the next section, we conducted walking experiments by using the non-adaptive and adaptive balance control strategy.

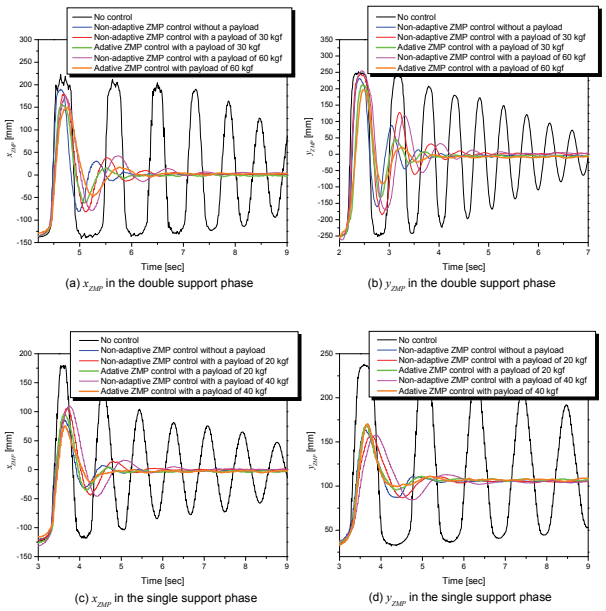

Fig. 7. Experimental results of ZMP control with payloads

TABLE II
APPROXIMATE SETTLING TIME IN THE DOUBLE SUPPORT PHASE

	Non-adaptive ZMP control without a payload	Non-adaptive ZMP control with a payload of 30 kgf	Non-adaptive ZMP control with a payload of 60 kgf	Adaptive ZMP control with a payload of 30 kgf	Adaptive ZMP control with a payload of 60 kgf
Settling time of x_{ZMP} control in DSP	1.9 [sec]	2.4 [sec]	2.9 [sec]	1.8 [sec]	1.9 [sec]
Settling time of y_{ZMP} control in DSP	2.1 [sec]	2.9 [sec]	3.4 [sec]	2.0 [sec]	2.1 [sec]

TABLE III
APPROXIMATE SETTLING TIME IN THE SINGLE SUPPORT PHASE

	Non-adaptive ZMP control without a payload	Non-adaptive ZMP control with a payload of 20kgf	Non-adaptive ZMP control with a payload of 40kgf	Adaptive ZMP control with a payload of 20 kgf	Adaptive ZMP control with a payload of 40 kgf
Settling time of x_{ZMP} control in SSP	2.2 [sec]	2.9 [sec]	3.6 [sec]	2.1 [sec]	2.1 [sec]
Settling time of y_{ZMP} control in SSP	2.4 [sec]	3.1 [sec]	3.9 [sec]	2.5 [sec]	2.6 [sec]

V. WALKING EXPERIMENTS

In this section, we describe the walking experiments in which we illustrated the effectiveness of the proposed walking pattern generation and balance control for variable passenger weights. As the passengers of the HUBO FX-1 can be categorized into either children or adults, the walking performances were compared and analyzed with payloads of 20 kgf, 40 kgf, and 60 kgf. After the payload was loaded into the cockpit, the force/torque sensor measured the payload, and then the equivalent pendulum lengths of the single and double support phases for the ZMP control were calculated. After this, the walking pattern was generated according to the calculated equivalent pendulum length of the single support phase and the predefined ZMP reference trajectory. Finally, the balance control inputs were superimposed onto the generated walking pattern during walking.

The walking experiments were conducted on a normal room floor with a local slope of approximately ±2 degrees. During the walking experiments, we collected the ZMP trajectories and body inclinations so as to compare the walking performances between the non-adaptive and adaptive cases. The walking parameters used in this experiment are as follows: step time = 1.0 second, step length = 250 mm, max. lift of the swing foot = 40 mm, and double support ratio = 5%. First, we performed walking experiments for the non-adaptive case in order to reproduce the walking performance of our previous research [5]. Hence, walking patterns and balance control gains were obtained by considering only the robot weight. We applied payloads of 20 kgf, 40 kgf, and 60 kgf, respectively. Similarly, we also performed walking experiments with the adaptive walking pattern and adaptive balance control. We applied payloads of 20 kgf, 40 kgf, and 60 kgf, respectively. Table IV details the RMS (root mean square) values of the ZMP tracking errors and body inclinations for both cases. It can be known that the ZMP tracking errors and body inclinations of the non-adaptive cases increased as the payload increased, while the walking performances of the adaptive cases maintained their performance in spite of the payload change. The RMS values of the x_{ZMP} and y_{ZMP} errors for the adaptive case were reduced by approximately 23% and 30%, respectively on the average. In addition, the RMS values of the rolling and pitching body inclinations for the adaptive case were also reduced by approximately 44% and 14%, respectively on the average. These results indicate that the HUBO FX-1 walked more stably with the adaptive walking pattern and balance control. For reference, Fig. 8 shows the comparison of ZMP trajectories and body inclinations between non-adaptive and adaptive cases with a payload of 60 kgf. A short video of the walking experiment can be seen on the web site, http://www.hubolab.com (Fig. 9). Thus, we were able to show the effectiveness of the proposed algorithm using walking experiments with the HUBO FX-1.

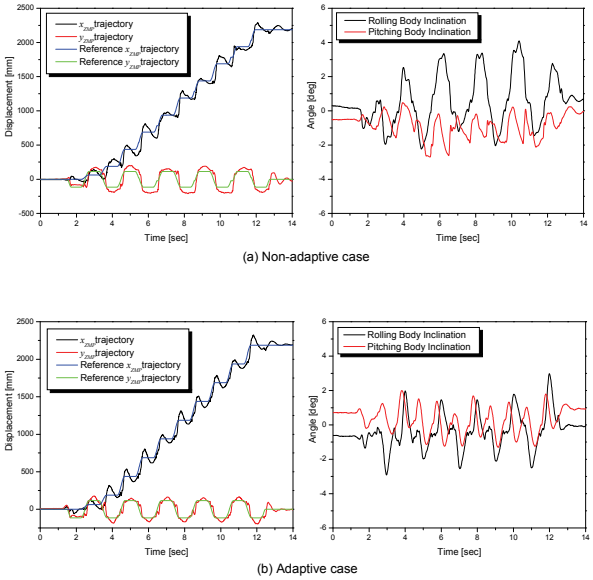

Fig. 8. Comparison of ZMP trajectories and body inclinations between non-adaptive and adaptive cases with a payload of 60 kgf.

TABLE IV
RMS VALUES OF ZMP TRACKING ERRORS AND BODY INCLINATIONS FOR EACH CASE

	Payload [kgf]	RMS value of x_{ZMP} error [mm]	RMS value of y_{ZMP} error [mm]	RMS value of rolling body inclination [deg]	RMS value of pitching body inclination [deg]
Non-adaptive case	20	40.39	54.56	1.57	0.82
	40	58.85	55.12	1.06	1.0
	60	56.92	56.39	1.35	0.91
Adaptive case	20	36.79	40.55	0.6	0.83
	40	36.64	38.88	0.72	0.63
	60	46.93	36.47	0.89	0.87

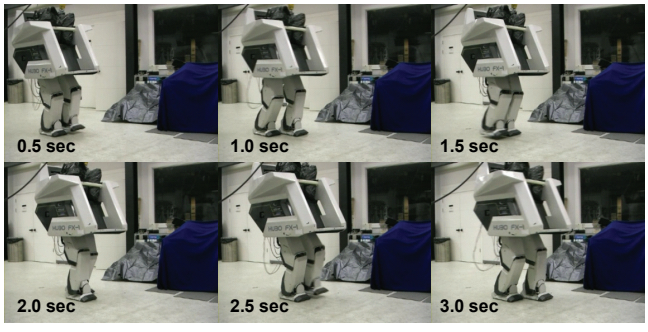

Fig. 9. Snapshot of the HUBO FX-1 forward walking with a payload of 60 kgf.

VI. CONCLUSION

This research focused on the adaptive walking pattern generation methods and balance control algorithms for the passenger-carrying biped robot, HUBO FX-1, for variable passenger weights. Our previous research [5] on the HUBO FX-1 has several drawbacks in that the walking patterns were experimentally obtained by trial and error, and the control gains of the balance controllers were selected by considering a constant passenger weight of 81 kgf. Using our previous method [5], the walking performance would decrease when a passenger weighed more or less than the predefined passenger weight. In order to solve this problem, this paper proposed a method to preserve the walking performance by changing the walking pattern and control gains depending on the passenger weight. Therefore, the previous ZMP controller was improved through the use of the variable state feedback gains that were easily calculated after measuring the passenger weight from force/torque sensors and calculating the equivalent length l. For the adaptive walking pattern generation, we used the convolution sum method [6]. Since this method contains the analytic weighting function of the equivalent length l, it can effectively calculate the walking pattern for variable passenger weights. Finally, the walking performances in the adaptive control method and the previous non-adaptive control method were quantitatively analyzed in terms of the ZMP and inclination for various passenger weights on the HUBO FX-1. The experimental results verified that the proposed adaptive method enables a better walking performance for different passenger weights.

REFERENCES

[1] Y. Sugahara, H. Lim, T. Hosobata, Y. Mikuriya, H. Sunazuka, and A. Takanishi, "Realization of dynamic human-carrying walking by a biped locomotor," in *Proc. IEEE Int. Conf. on Robotics & Automation*, pp. 3055–3060, 2004.

[2] Y. Sugahara, K. Hashimoto, M. Kawase, T. Sawato, A. Hayashi, N. Endo, A. Ohta, C. Tanaka, H. Lim, and A. Takanishi, "Walking pattern generation of a biped walking vehicle using a dynamic human model," in *Proc. IEEE/RSJ Int. Conf. on Intelligent Robots and Systems*, pp. 2497-2502, 2006.

[3] J. Chestnutt, P. Michel, K. Nishiwaki, J. Kuffner, and S. Kagami, "An intelligent joystick for biped control," in *Proc. IEEE Int. Conf. on Robotics & Automation*, Orlando, FL, pp. 860–865, 2006.

[4] Toyota, "Toyota.co.jp –news release-," December 2004. [Online]. Available: http://www.toyota.co.jp/en/news/04/1203_1d.html.

[5] J. Y. Kim, J. Lee, and J. H. Oh, "Experimental realization of dynamic walking for a human-riding biped robot, HUBO FX-1," *Advanced Robotics* **21**(3), 461–484, 2007.

[6] J. H. Kim, "Walking pattern generation of a biped walking robot using convolution sum," in *Proc. IEEE-RAS Int. Conf. on Humanoid Robots*, pp. 539–544, 2007.

[7] S. Kajita, F. Kanehiro, K. Kaneko, K. Fujiwara, K. Harada, K. Yokoi, and H. Hirukawa, "Biped walking pattern generation by using preview control of zero-moment point," in *Proc. IEEE Int. Conf. on Robotics& Automation*, pp. 1620–1626, 2003.

[8] K. Nagasaka, H. Inoue, and M. Inaba, "Dynamic walking pattern generation for a humanoid robot based on optimal gradient method," in *Proc. IEEE Int. Conf. on Systems, Man, and Cybernetics*, pp. 908–913, 1999.